International Journal of GEOMATE, July, 2017, Vol.13, Issue 35, pp.1- 7
Geotec., Const. Mat. & Env., ISSN:2186-2990, Japan, DOI: http://dx.doi.org/10.21660/2017.35.6698

EVALUATING THE RELATIONSHIP BETWEEN DYNAMIC SHEAR MODULUS AND NANO SCALE MODULUS OF ASPHALT BINDERS AT DIFFERENT AGING CONDITIONS

*Hasan M. Faisal[1], Umme A. Mannan[2], Rafiqul A. Tarefder[3], and Md Arifuzzaman[4]
[1,2]PhD Candidate and Graduate Research Assistant, University of New Mexico, USA
[3]Professor of Civil Engineering, University of New Mexico, USA
[4]Assistant Professor, Department of Civil Engineering and Architechture, University of Bahrain, Bahrain

*Corresponding Author, Received: 15 June 2016, Revised: 12 July 2016, Accepted: 22 Nov. 2016

ABSTRACT: Traditionally, asphalt binder is characterized by a dynamic shear rheometer, which applies a shear load on a bulk volume of liquid asphalt binder to determine shear modulus (G^*). Recently, a nanoindentation test can characterize an asphalt binder film in the form of a coating around roadway aggregates, which is more practical. In a nanoindentation test, a sharp tip is used to indent an asphalt film while residing on an aggregate surface to determine nanoindentation modulus (E). This study evaluates whether there is a relation between G^* and E. For both tests, replicate samples were conditioned in three ways: unaged, rolling thin film oven aged, and pressure vessel aging. Results show that the E-value is approximately 2 to 6 times larger than the G^*-value based on all samples/conditioning.

Keywords: Nanoindentation, Asphalt, Aging, Modulus, Binder, Dynamic, Shear.

1. INTRODUCTION

Asphalt concrete's (AC's) dynamic modulus (E^*) is one of the key input parameters for the structural design of flexible pavement according to the Pavement Mechanistic-Empirical Guide currently packaged as DARWin-ME software. Asphalt binder shear modulus G^*-based Witczak equation is used in pavement ME Level 2 analysis to estimate E^* of asphalt concrete from Hot Mix Asphalt (HMA) mix volumetrics and binder information. Specifically, asphalt binder's dynamic shear modulus (G^*) and phase angle (δ) are used in G^*-based Witczak equation to predict E^* mastercurve at Level 2 pavement ME analysis.

While AC's E^* testing is conducted using an axial compression (or tension), asphalt binder's G^* is conducted in shear mode [1-6]. Over the years, test methods developed and performed to characterize asphalt binders have been limited to a few rheological tests. Moreover, the existing tests cannot be performed on asphalt binder film while they are integral parts of AC. Rather, those tests are performed on bulk liquid asphalt separately. Nanoindentation has created an opportunity to determine the stiffness (E) of asphalt binder while they are parts of AC and under compression loading [7-11].

To this end, this study conducts G^* and E testing of selected Performance Grade (PG) asphalt binders from New Mexico sources. In addition, this study examines possible correlation between G^* and E. It is expected that asphalt binder's E will be a better estimator of asphalt concrete's E^* for Level 2 Pavement ME analysis.

2. THEORY OF NANOINDENTATION

A typical nanoindentation load displacement curve is shown in Fig. 1(a). A sitting load of 0.005 mN is typically applied initially to facilitate a contact between the tip and the sample's surface. Next, the load is increased gradually from point a to b. The tip is unloaded at the maximum load point b. The unloading path is assumed to be elastic for most of the elastoplastic material. The unloading curve does not come back to point a due to the plastic deformation in elastoplatic materials. The slope of the unloading curve at point b is usually equal to the slope of the loading curve at point a.

Fig. 1(b) shows the surface profile as a function of penetration depth during loading and unloading. Here, h_{max} is the total depth of indentation at a maximum load, h_p is the total depth of indentation that is unrecovered, h_s is the depth of the surface at the perimeter of the indenter contact and h_c is the vertical depth along which contact is made between the indenter and the sample. Therefore,

$$h_c = h_{\max} - h_s \quad (1)$$

The depth of impression that is recovered is,

$$h_e = h_{\max} - h_p \quad (2)$$

Hertz found the contact radius a is related to the indenter radius R, applied load P and the reduced elastic modulus E^* of a sample by (Fig. 2):

$$a^3 = \frac{3}{4}\frac{PR}{E^*} \tag{3}$$

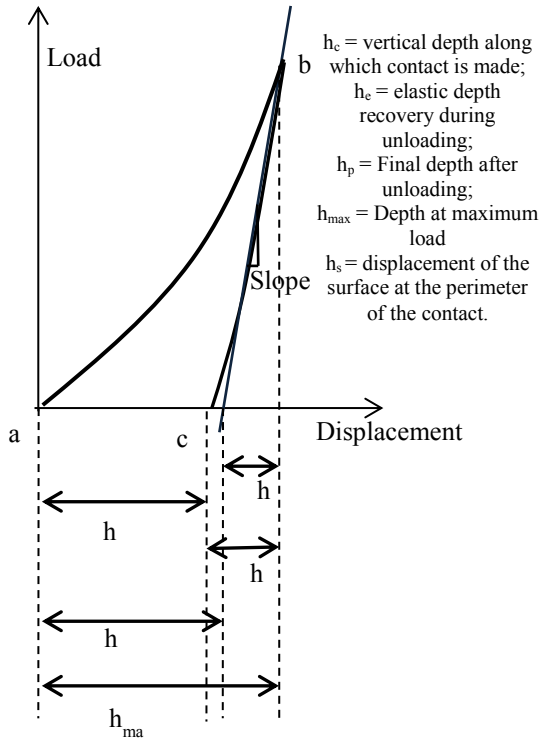

(a) Load –displacement curve

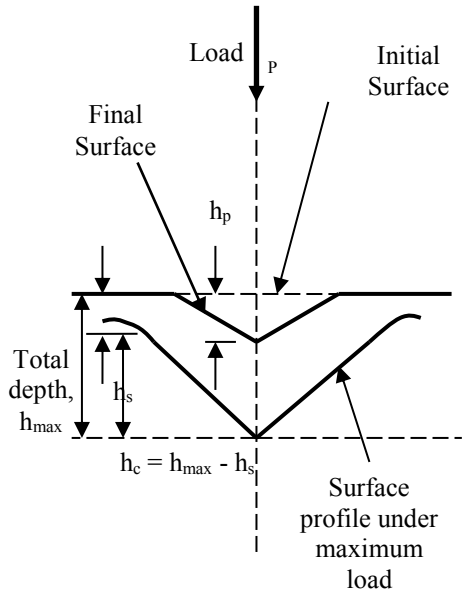

(b) Indentation Depth

Fig. 1 Schematic of Indentation Test

Contact radius a is also related to the indenter radius R and penetration depth by:

$$a = \sqrt{Rh} \tag{4}$$

From Eq. (2) and (3) the applied load can be written as:

$$P = \frac{4}{3}E^* R^{1/2} h^{3/2} \tag{5}$$

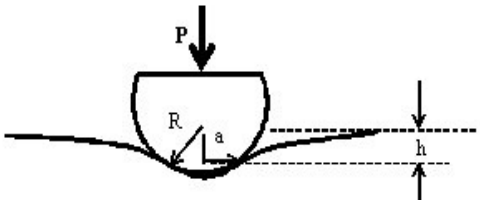

Fig. 2 Indenter Geometry

2.1 Determination of E^*

By differentiating Eq. (5) with respect to the penetration depth h. Using the relation in Eq. (4):

$$\frac{dP}{dh} = 2E^*\sqrt{Rh} = 2E^* a \tag{6}$$

The projected area at the maximum load can be defined as: $A = \pi a^2$
Therefore,

$$S = \frac{dP}{dh} = \frac{2}{\sqrt{\pi}}E^*\sqrt{A} \tag{7}$$

where S is the unloading stiffness or slope of the unloading curve, therefore,

$$E^* = \frac{\sqrt{\pi}}{2\sqrt{A}}(S) \tag{8}$$

Oliver and Pharr [12] used a power law function to fit the unloading path of the load-displacement curve [12]. The power law function used by Oliver-Pharr is shown in Eq. (9):

$$P = \alpha(h - h_f)^m \tag{9}$$

where h is the depth of penetration, h_f is plastic depth, α and m are curve fitting parameters related to tip geometry.

m = 1 for flat ended cylindrical tip, m = 1.5 for spherical tip, and m = 2 for conical tip (Berkovich tip). The slope is measured by differentiation the in above Eq. (9) at the onset of unloading.

2.2 Determination of *A*

Oliver and Pharr [12] defined the projected area *A* as a function of h_c defined in Eq. (1). Oliver and Pharr extrapolated the tangent line to the unloading curve at the maximum loading point down to zero load. This yields an intercept value for depth which estimates the h_s by:

$$h_s = \varepsilon \frac{P_{\max}}{S} \tag{10}$$

Therefore,

$$h_c = h_{\max} - \varepsilon \frac{P_{\max}}{S} \tag{11}$$

where $\boldsymbol{\varepsilon}$ is a geometric constant.
$\varepsilon = 0.72$ for conical tip, $\varepsilon = 0.75$ for Berkovich tip, and $\varepsilon = 0.72$ for spherical tip.

2.3 Determination of *E*

Timoshenko and Goodier [12] found the reduced elastic modulus, E^* is related to the modulus of the indenter and the specimen and given by:

$$\frac{1}{E^*} = \frac{1-\nu^2}{E} + \frac{1-\nu_i^{\,2}}{E_i} \tag{12}$$

where E is Young's modulus of the material,
$\boldsymbol{\vartheta}$ is Poisson's ratio of the material,
$\boldsymbol{E_i}$ is Young's modulus of the indenter,
$\boldsymbol{\vartheta_i}$ is Poisson's ratio of the indenter and
$\boldsymbol{E^*}$ is the reduced modulus. One can find the elastic modulus of the sample, E using Eq. (12).

2.4 Determination of *H*

Hardness, *H,* is defined by the maximum load divided by the projected area:

$$H = \frac{P_{\max}}{A} \tag{13}$$

where P_{max} = peak load and A = projected area of contact at the peak load. The unit of hardness is given in N/m^2=Pa.

3. MATERIALS AND SAMPLE PREPARATION

3.1 Collection

A total of four PG binders available in New Mexico were collected in five one-gallon buckets per PG binder. Asphalt binders used in the current study are PG 58-22, PG 64-22, PG 70-22 and PG 76-22.

Some performance graded asphalt binder such as PG 58-34, PG 64-34, PG 70-34 are not used in New Mexico. These binders could not be collected.

3.2 Conditioning

PG binders were subjected to three types of conditioning: (1) unaged/ original binder, and (2) RTFO (Rolling Thin Film Oven), and (3) PAV (Pressure Aging Vessel) aged before DSR testing. The RTFO Test simulates the short-term aging of asphalt binders that occurs during the hot-mixing process. The asphalt binder was exposed to an elevated temperature to simulate manufacturing and placement aging according to AASHTO T 240-09 test procedure [13]. Unaged asphalt binder was taken in cylindrical glass bottles and placed in a rotating carriage which rotates in the oven at 163 °C temperature for 85 minutes. After the RTFO aging, 50 gm sample was placed in the PAV plate and then aged at 100 °C and 2.10 MPa for 20 hours according to the AASHTO R 28-12 [14]. Fig. 3 shows the PAV apparatus.

Fig. 3 Pressure Aging Vessel (PAV) for long term aging simulation on asphalt binder

3.3 Nanoindentation Sample Preparation

Fig. 4 shows a laboratory prepared asphalt binder film on glass substrate. As the first step, a glass slide surface 0.5 in. × 0.5 in. was selected and weighed in scale up to 4 significant decimal digits of grams. Next, the glass slide was wrapped with high temperature resistant tape. The tape was placed so that it formed the 0.25 in. square gap area previously outlined for the binder. Then, hot polymer modified liquid asphalt binder was poured into the gap between the tape strips. The polymer-modified binders were melted by heating them to 163 °C for an hour. The asphalt coated surface was placed in the oven at 163 °C for 10 min. in order to have a smooth surface, cooled at room temperature and the tapes were

removed. Finally, the glass slide with the asphalt coating was weighed again to measure the amount of asphalt binder. From the known area, the density of the asphalt binder and mass of the binder film was measured. The film thickness varied within a range of 40 µm to 80 µm to avoid the substrate effect on the test results.

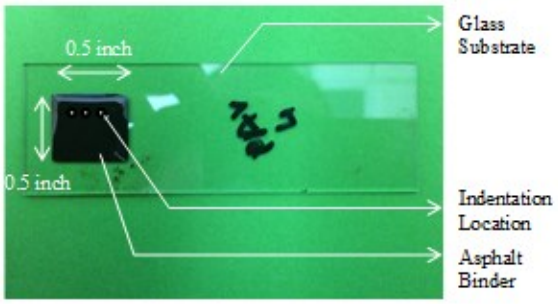

Fig. 4 Asphalt Binder Sample for Nanoindentation

4. TESTING

4.1 Dynamic Shear Rheometer (DSR) Testing

Dynamic Shear Rheometer (DSR) was conducted on the conditioned binders. The test measures the dynamic shear modulus or complex modulus, G^* and phase angle, δ of asphalt binders under a continuous sinusoidal loading using a DSR and parallel plate test geometry. Fig. 5 shows the DSR test device. The G^* and δ were measured at room temperatures and a loading frequency of 10 rad/sec. A thicker sample (2 mm) with a smaller diameter plate (8 mm) was used so that the phase angle (δ) became measurable. All the tests were conducted following the AASHT0 T 315-09 [15] test protocol within the linear viscoelastic range under strain-controlled mode. Three replicate samples were tested and the average of the three tests was used to develop the master curve.

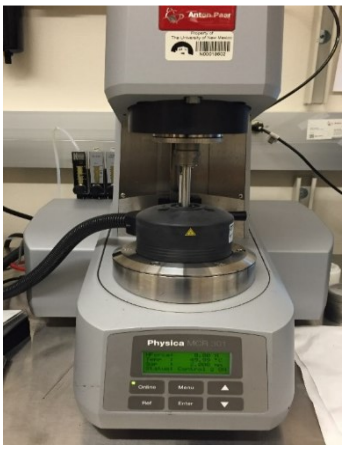

Fig. 5 Dynamic Shear Rheometer

4.2 Nanoindentation Testing

Indentation experiments were performed by using a nanoindenter manufactured by MicroMaterials Ltd. in Wrexham, UK. In all the tests, the nanoindenter was equipped with the pyramidal Berkovich tip. The indentation tests were conducted in load control mode. In load control mode, the indentation includes a constant loading, unloading rate and a holding segment at maximum load. A maximum load of 0.055 mN was applied with an initial load of 0.005 mN. Thirty indentations for loading rate 0.002 mN/sec, unloading rate 0.002 mN/sec and dwell time of 200 sec. were selected. The loading, unloading rate and dwell times were selected so the tests could be performed in the thin film without hitting the glass substrate, according to the study of Tarefder and Faisal [8]. The indentation depth remained small compared to the total material thickness so that the substrate effect on determining the mechanical property of the material could be avoided. The indenter moved at a rate of 1µm/sec to make the initial contact. In all the tests, the camber test temperature was kept at 26 ˚C, within a fluctuation of ±0.2 ˚C. After the test, the temperature corrections were also provided to the analysis. In the test, for each sample a set of 5 indentations (see Fig. 6) were made on the sample with a distance of 300 µm. The distance was selected to avoid the pile up and sink in effect for successive indentations. However, according to ASTM guidelines [16], the required distance needed to be at least six indent radii away from the previous indentation point. Because of the soft bulk of the asphalt binder, the pile up effect could be more. Furthermore, there was no limitation of space in the sample in nanoscale. For these reasons, a substantial distance was chosen for testing the material. Three different aging conditions of the asphalt binder samples were introduced and 20 indentations were conducted for each sample.

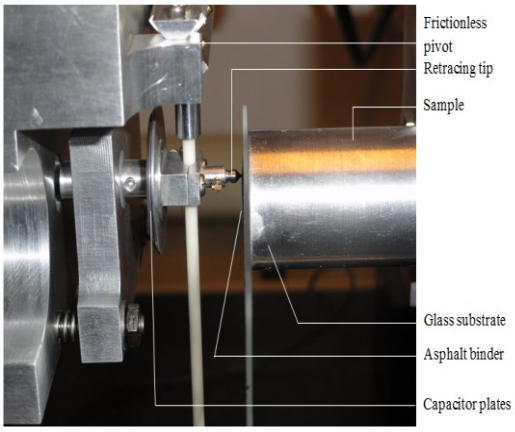

Fig. 6 Nanoindentation on unaged sample

5. RESULTS AND DISCUSSIONS

In the current study, a comparative analysis was conducted between complex modulus of the binder G^* and nanoindentation modulus E of the material.

Figure 7 shows the complex modulus G^* of four different binders and three different types of aging conditioning. The figure shows that with an increase in aging the complex modulus of the binder increases, however, the increase is comparatively higher for PAV conditioning. Since PAV conditioning simulates long term aging in asphalt binder, the complex modulus is almost 3 to 5 times higher for PAV conditioning, however that is for RAFO conditioning is only 1.1 to 1.9 times higher.

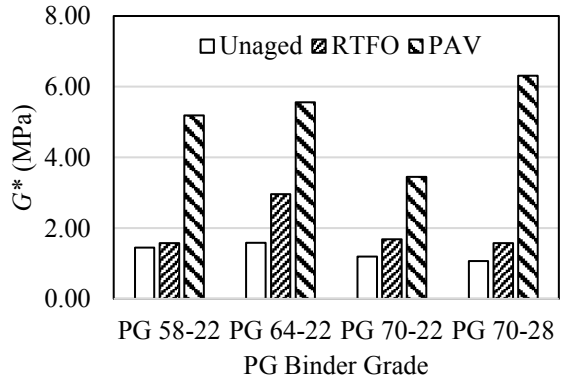

Fig. 7 G^* of different PG grades and three different types of conditioning

Figure 8 shows the load displacement curves obtained from unaged PG 70-22 asphalt binder. Twenty indentations are conducted on each binder sample. The load displacement curve shows maximum displacement is restricted to 7200 nm.

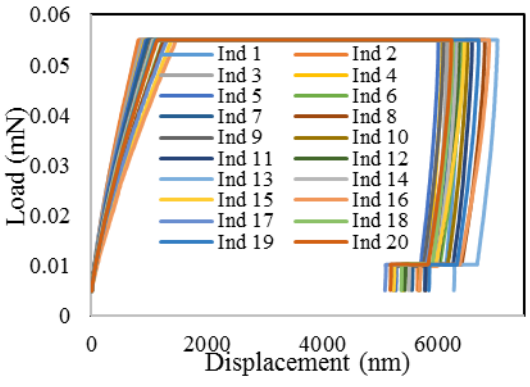

Fig. 8 Load displacement behavior of PG 70-22 unaged asphalt binder

The selected high unloading rate and extended dwell time made the unloading portion of the load displacement curve positively sloped. Therefore, it was possible to analyze the unloading data in Oliver-Pharr [12] framework. Figure 9 shows the modulus determined from nanoindentation test. Results again show the modulus of the material increases with increase in aging condition of asphalt. The increase in modulus is 4 to 8 times higher in the case of RTFO conditioning, however it is 10 to 23 times for PAV conditioning. Therefore, for all cases of the nanoindentation modulus E is found higher than the complex modulus G^* of the material at room temperature and 10 rad/sec frequency. Comparison between E and G^* shows nanoindentation E of the material is 1.5 to 6 times higher than the G^* of the material. However, the increase in the factor n $(=E/G^*)$ shows a decreasing trend for PAV aging conditioning of PG 58-22 and PG 70-28.

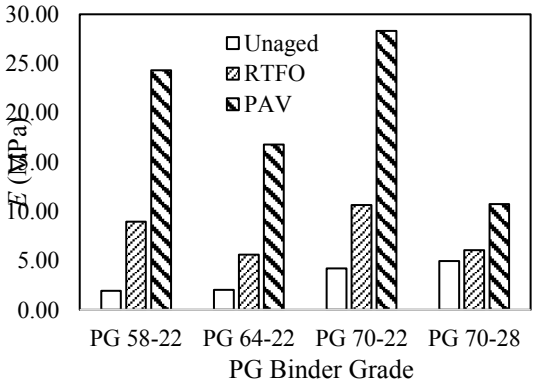

Fig. 9 E from nanoindentation test for different PG binder grade and aging conditioning

E might had showed higher values compared to the G^* of the material. Since both of these binders are manufactured with polymer modification in the binder industry, the polymer structure may reduce the effect of aging on the nano scale structure of the binder material.

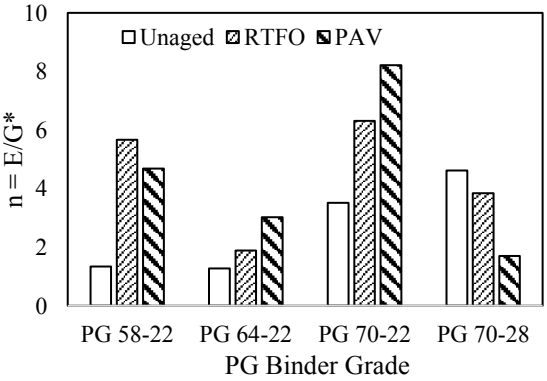

Fig. 10. n-value comparison for different PG binder grade and aging condition

6. CONCLUSION

The following conclusions can be drawn from the current study:

i) Both complex modulus and nanoindentation modulus increases with an increase in the aging conditioning of the material.

ii) Nano scale modulus of the binder is 2 to 6 times higher than micro scale modulus or complex modulus of the material irrespective of the aging conditioning.

iii) Nano scale modulus increases 4 to 8 times for RTFO aging conditioning where micro scale modulus shows an increase of 10 to 23 times for PAV aging conditioning with respect to the unaged asphalt binder.

7. ACKNOWLEDGEMENTS

The authors would like to express their sincere gratitude and appreciation to the Safety and Operations of Large-Area Rural/Urban Intermodal Systems (SOLARIS), a tier 1 university transportation center led by the University of Nevada, Reno, for providing the funding for this research project.

8. REFERENCES

[1] Guddati M, Feng Z, and Kim Y, "Toward a micromechanics-based procedure to characterize fatigue performance of asphalt concrete", Transportation Research Record: J. of the Transportation Research Board, No. 1789, 2002, pp. 121–128.

[2] Little D.N., Letton A, Prapnnachari S, and Kim Y.R., "Rheological and rheo-optical characterization of asphalt cement and evaluation of relaxation properties", Transportation Research Record, No. 1436, 1994, pp. 71–82.

[3] Xu Q, and Solaimanian M, "Modelling linear viscoelastic properties of asphalt concrete by the Huet--Sayegh model", International J. of Pavement Engineering, Vol. 10, No. 6, 2009, pp. 401–422.

[4] Buttlar W, and You Z, "Discrete element modeling of asphalt concrete: microfabric approach", Transportation Research Record: J. of the Transportation Research Board, No. 1757, 2001, pp. 111–118.

[5] Djakfar L, Bowoputro H, Akbariawan R, and Fadiansyah R, "The effect of limestone and reheating temperature on cold paving hot mix asphalt", International J. of GEOMATE, Vol. 12, No. 29, pp. 212–219.

[6] Sas W, Glucowski A, and Szymanski A, "The geotechnical properties of recycled concrete aggregate with addition of rubber chips during cyclic loading", International J. of GEOMATE, Vol. 12, No. 29, pp. 25–32.

[7] Faisal H.M., Tarefder R, and Weldegiorgis M, "Nanoindentation characterization of moisture damage in different phases of asphalt concrete", Advances in Civil Engineering Materials, Vol. 4, No. 1, 2015, pp. 31–46.

[8] Tarefder R.A., and Faisal H, "Effects of dwell time and loading rate on the nanoindentation behavior of asphaltic materials", J. of Nanomechanics and Micromechanics, ASCE, Vol. 3, No. 2, 2013, pp. 17–23.

[9] Tarefder, R.A., and Faisal, H. M., "Nanoindentation characterization of asphalt concrete aging", J. of Nanomechanics and Micromechanics, ASCE, 2013, Vol. 4, No.1, 2013 A4013003.

[10] Tarefder, R.A., and Faisal, H. M., "Modeling nanoindentation creep behavior of asphalt binder", Advances in Civil Engineering Materials, ASTM, Vol. 2, No.1, 2013, pp. 418–440.

[11] Faisal H.M., Tarefder R.A., and Hossain M.I., "A nanomechanical characterization of vapor condition and unconditioned asphalt", Transportation Research Record: J. of the Transportation Research Board, No. 2506, Transportation Research Board, Washington, D.C., 2015, pp. 126–136, DOI: 10.3141/2506-14.

[12] Oliver, W.C., and Pharr G.M., "An improved technique for determining hardness and elastic modulus using load and displacement sensing indentation experiments", J. Materials Research, 1992, Vol. 7, No.6, pp.1564–1583.

[13] AASHTO Standard T240 – 09, Standard Method of Test for Effect of Heat and Air on a Moving Film of Asphalt (Rolling Thin-Film Oven Test), American Association of State and Highway Transportation Officials, 2013, Washington, DC.

[14] AASHTO Standard R28-12, Standard Practice for Accelerated Aging of Asphalt Binder Using a Pressurized Aging Vessel (PAV), American Association of State and Highway Transportation Officials, 2013, Washington, DC.

[15] AASHTO Standard R315-09, Standard Method of Test for Determining the Rheological Properties of Asphalt Binder Using a Dynamic Shear Rheometer (DSR), American Association of State and Highway Transportation Officials, 2013, Washington, DC.

[16] ASTM Standard E2546 – 07, Standard Practice for Instrumented Indentation Testing, ASTM International, West Conshohocken, PA, DOI: 10.1520/E2546-07, www.astm.org.